Journal of Hazardous Materials 179 (2010) 444–452

Contents lists available at ScienceDirect

Journal of Hazardous Materials

journal homepage: www.elsevier.com/locate/jhazmat

Gold and gold–iron modified zeolites—Towards the adsorptive deodourisation

Izabela Sobczak[a,*], Hubert Pawlowski[a], Jaroslaw Chmielewski[b], Maria Ziolek[a]

[a] A. Mickiewicz University, Faculty of Chemistry, Grunwaldzka 6, 60-780 Poznan, Poland
[b] Poznan University of Economics, Faculty of Commodity Science, al. Niepodległości 10, 61-875 Poznan, Poland

ARTICLE INFO

Article history:
Received 1 December 2009
Received in revised form 20 February 2010
Accepted 7 March 2010
Available online 12 March 2010

Keywords:
Y, Beta and ZSM-5 zeolites
Au, Fe modification
Acidity
Adsorption of Bu_2S
E-nose

ABSTRACT

Zeolites exhibiting different structures (Y, Beta, and ZSM-5) were modified with gold and iron and applied for odour adsorption from the air containing dibutyl sulphide (Bu_2S) used as a representative odour producing compound. The structure of the zeolites used determines the rate of adsorption (higher on Y type zeolites and smaller on two other zeolites), whereas hydrophilicity affects the selectivity towards Bu_2S adsorption increasing in the order: Y < Beta < ZSM-5. For the same zeolite structure, Bu_2S adsorption selectivity depends on the total acidity of zeolites which increases after iron modification. The texture and surface properties of the modified zeolites were studied by XRD, XPS, UV–vis, TEM, pyridine adsorption and FTIR, test reactions (acetonylacetone cyclisation, isopropanol decomposition).

1. Introduction

Odour pollution of the atmosphere is a common environmental problem. In particular, much effort has been made to limit odour emissions from the agriculture and food industries. The treatment of gas emissions is an important measure to protect both public health and the environment. Long term exposured odours are often removed by biological units. However, they are not sufficient for the reduction of malodours below the odour threshold. To reduce the concentrations below odour threshold, selective adsorption processes with on-site regeneration of the adsorbents are very promising [1]. Looking for the selective adsorbents one should take into account the nature of odour compounds (most of them are organic compounds containing nitrogen and/or sulphur) and the nature of elements (located on the surface of sorbents) that are actively involved in selective adsorption.

Our former study has shown [2–4] that the high pore volume nanomaterials (Y zeolites and mesoporous MCM-41) modified with active components (e.g. Ni, Cu, Mn, Au) are able to concentrate high amount of pollutants in a minimum volume of solids. Butyl amine ($BuNH_2$) and dibutyl sulphide (Bu_2S) were adsorbed on these materials in the presence and absence of humid atmosphere and it was found that transition metal exchanged zeolites reveal higher selectivity towards amine adsorption than that towards sulphide adsorption, contrary to Au containing MCM-41 mesoporous materials which are more selective in sulphide adsorption. Moreover, it was evidenced that nickel containing sorbents are easily regenerated via catalytic oxidation of adsorbates [4]. The most attractive adsorbents of amines and sulphides found in our previous study were gold modified MCM-41 materials which not only adsorb the highest amounts of both odours but also are highly selective in competition with moisture adsorption. Niobium located in NbMCM-41 matrix enhances the hydrophobicity of the material and increases the adsorption of odour at high concentration of water vapour.

Ordered mesoporous materials are not very stable and their properties change with the time of use. Therefore, in this work we modified three different types of zeolites (Y, Beta and ZSM-5 with different Si/Al ratio and hydrophobic/hydrophilic character) with iron and/or gold to obtain sorbents able to concentrate a maximum amount of odours in a minimum volume of adsorbents. The choice of active components was determined by the expected selectivity towards sulphide adsorption and a possible further recovery of sorbent via the catalytic oxidation of odours at room temperature. Dibutyl sulphide (Bu_2S), used as a representative of odour compounds, was adsorbed on the materials prepared.

2. Experimental

2.1. Modification of the catalysts

2.1.1. Gold catalysts

NaY (Si/Al = 2.7, Katalistiks), H-Beta (Si/Al = 12.5, Süd Chemie, Germany) and H-ZSM-5 (Si/Al = 44.9, Süd Chemie, Germany)—types of zeolites were used in this research. The gold catalysts were prepared according to [5]: a 1250 ml volume of chloroauric acid ($HAuCl_4 \cdot 4H_2O$, Johnson Matthey, UK–USA) solution of 8.2×10^{-4} M

* Corresponding author. Tel.: +48 61 8291305.
E-mail address: sobiza@amu.edu.pl (I. Sobczak).

0304-3894/$ – see front matter © 2010 Elsevier B.V. All rights reserved.
doi:10.1016/j.jhazmat.2010.03.024

Table 1
Metal loadings and Si/Al ratios in zeolites.

Catalyst	Si/Al	Metal loading (wt.%)		Cation exchange (%)
		Fe	Au	Fe
Au-Y	2.7	–	0.59	–
Au/Fe-Y	2.7	7.88	1.00	97.9
Au-Beta	12.5	–	0.83	–
Au/Fe-Beta	12.5	1.09	1.00	48.5
Au-ZSM-5	44.9	–	0.1	–
Au/Fe-ZSM-5	44.9	0.29	1.00	43.5

was prepared, and its pH was adjusted to 6.0 by adding NaOH solution; after that 10 g of zeolite was added, the solution was heated to 353 K and stirred at this temperature for 16 h. The supported gold samples were obtained after filtration and washing, and then dried at 423 K. The gold content was analysed by ICP-MS. The results are summarized in Table 1.

2.1.2. Gold–iron catalysts

Iron was incorporated into zeolites by the ion exchange (IE) procedure. The Fe IE was performed by stirring of the solid in 0.05 M aqua solution of $Fe(NO_3)_3$ (Aldrich) at 308 K for 6 h. After stirring, the samples were filtrated, washed and dried at 373 K. For loading of gold, the incipient wetness impregnation procedure was applied [6]. The required amount of $HAuCl_4{\cdot}4H_2O$ (corresponding to 1 wt.% of Au) was dissolved in deionized water. This solution was always freshly prepared and was added dropwise to the Fe-containing support upon intense stirring. On completion of the addition, the support was slightly wet. The resulting catalysts were dried for 16 h at 353 K and then calcined for 3 h at 623 K. The iron and gold content was analysed by ICP-MS (Varian). The results are summarized in Table 1.

2.2. Catalysts characterisation

The XRD patterns were obtained on a D8 Advance diffractometer (Bruker) using CuK_α radiation ($\lambda = 0.154$ nm), with a step size of 0.05° in the $2\Theta = 6$–60° range.

The UV–visible spectra were recorded on a Cary 300Scan (Varian) spectrometer. Catalysts in the form of powders were placed in the cell equipped with a quartz window. The Kubelka–Munk ($F(R)$) was used to convert reflectance measurements into equivalent absorption spectra using the reflectance of SPECTRALON as a reference. The spectra were recorded in the range from 800 to 190 nm.

Photoemission spectra (XPS) were collected by a VSW Scientific Instrument spectrometer, equipped with a standard Al Kα excitation source. The binding energy (BE) scale was calibrated by measuring C 1s peak (BE = 285.1 eV).

For transmission electron microscopy (TEM) measurements the powders were deposited on a grid covered with a holey carbon film and transferred to JEOL 2000 electron microscope operating at 80 kV.

The surface properties were characterised by pyridine adsorption followed by FTIR spectroscopy and by test reactions—acetonylacetone (AcoAc) cyclisation and 2-propanol decomposition.

Infrared spectra were recorded with a Bruker Vector 22 FTIR spectrometer using an in situ cell. Samples were pressed under low pressure into a thin wafer of ca. 10 mg cm^{-2} and placed inside the cell. Catalysts were evacuated at 623 K for 3 h and pyridine (PY) was then admitted at 423 K. After saturation with PY the samples were degassed at 423, 473, 523 and 573 K in vacuum for 30 min. Spectra were recorded at room temperature in the range from 4000 to 400 cm^{-1}. The spectrum without any sample ("background spectrum") was subtracted from all spectra recorded. The IR spectra of the activated samples (after evacuation) were subtracted from those recorded after the adsorption of PY followed by various treatments. The spectra reported are the results of this subtraction.

A tubular, down-flow reactor was used in AcoAc cyclisation reaction that was carried out at atmospheric pressure, using nitrogen as the carrier gas. The catalyst bed (0.05 g) was first activated for 2 h at 623 K under nitrogen flow (40 cm^3 min^{-1}). Subsequently, 0.5 cm^3 of acetonylacetone (Fluka, GC grade) was passed continuously over the catalyst at 623 K. The substrate was delivered with a pump system and vaporized before being passed through the catalyst with the flow of nitrogen carrier gas (40 cm^3 min^{-1}). The reaction products were collected for 30 min downstream of the reactor in the cold trap (mixture of 2-propanol and liquid nitrogen) and analysed by gas chromatography (CHROM-5, Silicone SE-30/Chromosorb G column).

The 2-propanol conversion (dehydration and dehydrogenation) was performed, using a microcatalytic pulse reactor inserted between the sample inlet and the column of a CHROM-5 chromatograph. The catalyst bed (0.05 g) was first activated at 623 K for 2 h under helium flow (40 cm^3 min^{-1}). The 2-propanol (Aldrich) conversion was studied at 423, 473, 523 and 573 K using 3 μl pulses of alcohol under helium flow (40 cm^3 min^{-1}). The reactant and the reaction products: propene, 2-propanone (acetone) and diisopropyl ether were analysed using CHROM-5 gas chromatograph on line with microreactor. The reaction mixture was separated on 2 m column filled with Carbowax 400 (80–100 mesh) at 338 K in helium flow (40 cm^3 min^{-1}) and detected by TCD.

2.3. Adsorption of odours

Adsorption of the odour producing dibutyl sulphide (Bu_2S) was performed at room temperature and was evaluated by two methods, with the balance scale and an "electronic nose".

The outgased powdered sorbent (0.1 g of zeolite) was put on the balance scale in the glass box purged with air flow. In this box the 0.3 cm^3 of odour producing substance (Bu_2S) was evaporated and the amount of the compound adsorbed was continuously weighed and the course of the weight change was recorded by a computer program for 10 days. In the middle of this period another 0.3 cm^3 dose of dibutyl sulphide was injected into the box. The kinetic adsorption curves obtained under isotherm conditions were plotted on the basis of the weight changes. These curves represent the total adsorption (all adsorbates: Bu_2S, moisture, CO_2 and others from air are considered). Finally chemical analysis of the solids was performed that allow us to calculate the wt% of Bu_2S adsorbed on zeolites.

In the second system the phials painted inside by chalk paint with the addition of zeolite (10, 20 and 50 wt.%) or without the catalyst were used. A portion of 0.2 μl of dibutyl sulphide was injected into each phial. After injection, the phials were heated (5 h, 363 K) and then the atmosphere in the phials was analysed using an 20 mm Crimp-Cap with Septa Butyl (gray)/PTFE (BGB Analityk AG). The phials into which Bu_2S was not injected, were used as a reference material.

The electronic nose that enables analysis of samples containing volatile substances, even of complex composition, was applied for analysis of dibutyl sulphide and products of its transformation. The analyses of samples were performed using TurboMatrix HX40 headspace sampler and TurboMass Mass Spectrometer as a detector (both devices made by Perkin Elmer, Norwalk) which was controlled by chemometric software TMSOFT NT made by HKR Sensorsysteme, Munich.

Four replicates of each type of samples were analysed after thermostating step during 500 min at 318 and 363 K (separately analysed). Next, the headspace gas was injected by needle heated to

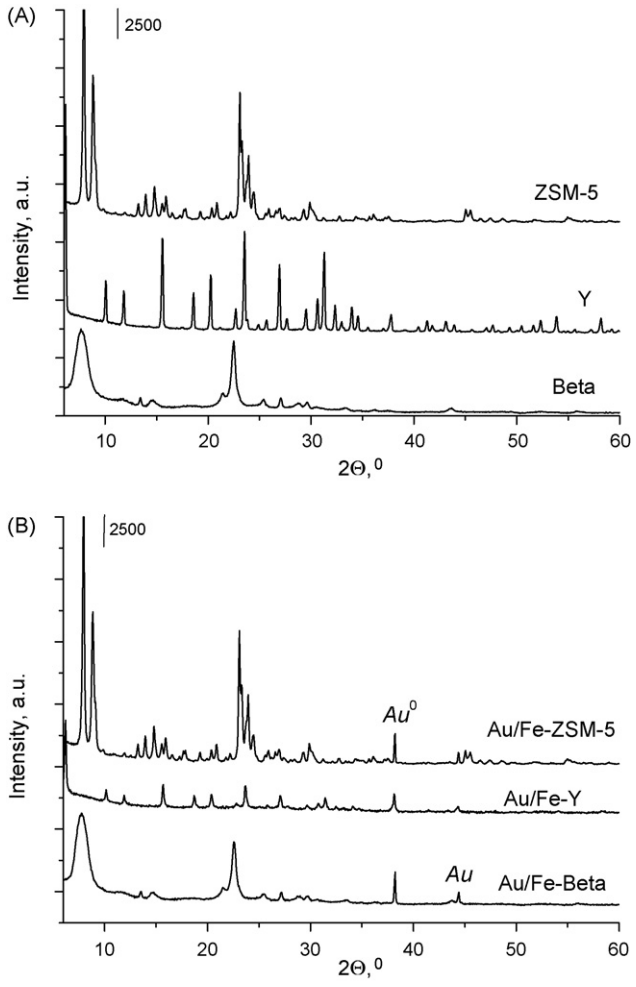

Fig. 1. XRD patterns of zeolites before (A) and after modification with Au and Fe (B).

373 K, into system, after 1 min pressurization of sample. Before next analysis the analytical system was purged during 20 min. Whole mixture of volatile components of each sample was introduced into the mass spectrometer detector, and the mass spectra of each sample were acquired in range 50–250 m/z, in the run: 30 s—zero level, 90 s—building-up and 30 s—signal level. Helium was used as carrier gas.

Entire mass spectra of volatile components were applied for analysis of dibutyl sulphide and products of its transformation.

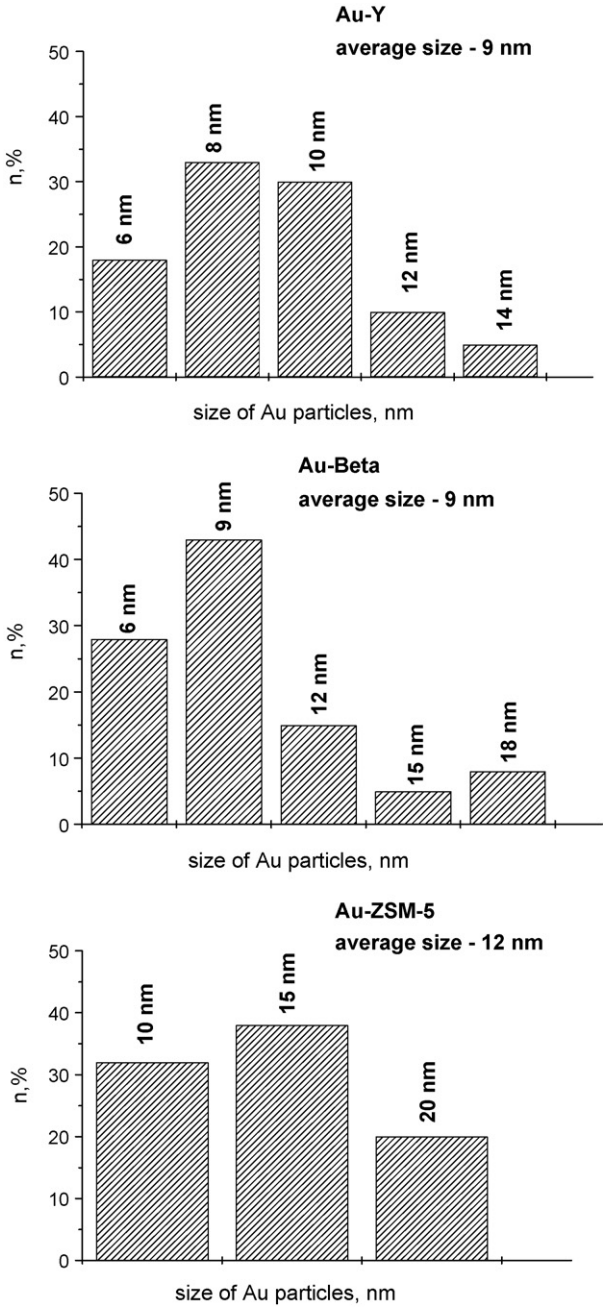

Fig. 2. Gold particles size distribution for Au-zeolites.

3. Results

3.1. Chemical composition and structure of zeolites

Table 1 presents the data on the Si/Al ratio and the metal loading in zeolites. Although the amount of gold in the solution during the modification was always the same (2 wt.%), the data clearly show that the amount of gold in the final gold-containing materials (Au-Y, Au-Beta and Au-ZSM-5) differed depending on the structure. The metal loading in all zeolites was much lower than assumed. The highest gold loading was found in Au-Beta zeolite, the lowest in Au-ZSM-5. It indicates that the gold introduction is the most effective in the structure of Beta zeolite.

As to the modification with iron, the total Fe cation exchange in zeolites (assuming Fe^{3+} oxidation state of exchanged cations) gave 8 wt.% of Fe in Fe-Y, 2.2 wt.% in Fe-Beta and 0.7 wt.% in Fe-ZSM-5. Iron exchanged zeolites were used as supports for gold introduced via impregnation. In the zeolites containing gold and iron, the iron content varied from the maximum possible exchange depending on the zeolite structure. Table 1 shows that in Y zeolite, 98% of its maximum exchange capacity was reached. It is very high amount suggesting that iron occupies not only cation-exchanged positions. Large cations, like iron ones, can hardly occupy cationic positions in hexagonal prisms in Y type zeolite, and for them the maximum exchange capacity is ca. 68%. Thus, it is supposed that the rest of iron species could be located in the framework positions (substituting Si or Al in the lattice) or in the form of bulk iron-oxide species. The lowest amount of iron was introduced into ZSM-5 structure. However, it is worthy of notice, that the degree of iron exchange is similar for zeolites Beta and ZSM-5 (between 40 and 50%). The loading of gold on the surface of iron containing zeolites by the impregnation method is equal to 1 wt.% for all zeolites used.

The XRD results of gold-containing catalysts (not shown here), with the diffraction peaks being characteristic of the Y, Beta and ZSM-5 structures, according to the data in [7], showed that the framework of parent zeolites is well preserved after deposition–precipitation and that all the zeolite structures were maintained after surface modification with gold. Similarly, the XRD patterns of Au/Fe-Beta and Au/Fe-ZSM-5 zeolites show typical diffraction peaks corresponding to the characteristic BEA and MFI structure [7], so the crystallinity of Beta and ZSM-5 zeolite was not altered by iron and gold incorporation. The exception is Au/Fe-Y, whose XRD pattern exhibits much weaker characteristic diffraction peaks at 2Θ = 6–60° in comparison with the diffractogram of the pristine NaY zeolite (Fig. 1). This difference may indicate some deterioration of the FAU structure after the iron exchange and subsequent impregnation with gold. Similar behaviour was shown in [8] for gold–iron modified Y zeolite where iron was introduced by impregnation and gold by cationic-exchange. The decrease in elementary unit of Au/Fe-Y (24.65 Å) compared with that of NaY (24.79 Å) is a result of sodium exchange for Fe (three Na^+ of 0.098 nm exchanged by one Fe^{3+} of 0.062 nm diameter).

3.2. Gold and iron species in zeolites

3.2.1. X-ray diffraction

In the 2Θ = 6–60° range of XRD patterns the reflections characteristic of metallic gold (at 2Θ = 38.2° and 44.8°) and iron oxides (at 2Θ = 33.2, 35.6, 40.9, 49.5) [8–10] could be identified.

In the XRD patterns of gold zeolites modified by deposition–precipitation (not shown here) the peaks corresponding to metallic gold were not detected because of too small content of gold (below 1 wt.%). The presence of metallic gold in these samples was found by UV–vis spectra, XPS and TEM techniques (see Sections 3.2.2–3.2.4).

In contrast, the XRD patterns of all Au-impregnated/Fe-containing samples (Fig. 1) clearly indicate the presence of metallic gold particles characterised by the reflections at 2Θ = 38.2° from Au (1 1 1) and at 44.8° from Au (2 0 0) [8,9]. The peaks assigned to Au are sharper in the patterns of Au/Fe-Beta and Au/Fe-ZSM-5 samples than in that of Au/Fe-Y suggesting bigger Au agglomerates located on Beta and ZSM-5 zeolites. Y zeolite modified with gold and Fe contains the highest amount of iron from among all materials studied. Most probably the strong interaction between iron cations and the precursor of gold makes Au stabilization stronger on active centres (iron cations playing the role of active centres for gold adsorption), which protects agglomeration of gold clusters. It is important to stress that the crystalline structures of iron oxides were not observed on gold–iron zeolites by XRD technique suggesting good dispersion of iron species on the internal/external surface and limited segregation of Fe_xO_y nanoparticles.

3.2.2. TEM

Fig. 2 presents the gold particles size distribution and the average diameter of gold nanoparticles supported on Y, Beta and ZSM-5 zeolites. The particle size distributions are similar on Au-Y and Au-Beta zeolites (the average diameter of gold particles is ca. 9 nm). Most of gold nanoparticles (ca. 60%) in Y zeolite are between 8 and 10 nm, while in Beta zeolite the fraction of gold particles about 9 nm (ca. 45%) dominates. However, it is worthy of notice that bigger gold particles (up to 14–18 nm) are also present in both samples. The particle size distribution of Au-ZSM-5 is more uniform, but the gold nanoparticles present on the surface of Au-ZSM-5 are bigger than those on Au-Y and Au-Beta. The average diameter of gold particles on Au-ZSM-5 is of ca. 12 nm. However, most of gold particles (ca. 40%) in Au-ZSM-5 exhibit ca. 15 nm diameter and the largest gold particles are of about 20 nm. Taking into account the sizes of cages/channels in the zeolites used (Y—ca. 1.2 nm, Beta—ca. 0.66 and 0.56 nm and ZSM-5—ca. 0.55 nm) it is clear that gold nanoparticles are located on the external surface of zeolites. However, one cannot exclude that very small Au particles are present inside the cavities/channels of zeolites.

Gold particles in TEM pictures of Au/Fe-Y, Au/Fe-Beta and Au/Fe-ZSM-5 zeolites exhibit various dimensions and shapes (especially for agglomerates), which makes it difficult to estimate their sizes. However, XRD results (Section 3.2.1) indicate that bigger gold crystallites are on the surface of gold–iron than gold zeolites. For Au–Fe samples the calcination at 623 K after gold impregnation leads to formation of gold particle agglomerations.

Table 2
XPS results.

Catalyst	Au4f [eV]
Bulk gold	84.0
Au-Y	83.15
Au-Beta	83.54
Au-ZSM-5	83.40

3.2.3. XPS

XPS results for Au-Y, Au-Beta and Au-ZSM-5 zeolites are presented in Table 2. It is known that the signal of Au^0 of bulk metal equals to 84.0 eV [11]. The data shown in Table 2 indicate that the binding energies of the Au4f peak obtained for gold zeolites shift to lower values (BE = 83.40–83.15 eV) in comparison with those in the reference bulk metal. The greatest shift towards lower binding energies was found for Au-Y zeolite. Such a negative shift has also been observed recently for gold-containing mordenite [12] and TiO_2 [13] and other supported gold catalysts [14,15] and has been attributed to the changes in electronic structure with increasing size of the gold particles deposited on the support [16] or to electron transfer from the support to the Au particle ($Au^{\delta-}$) [15,17,18]. The shift towards lower binding energies has also been observed for the catalysts pretreated with H_2 and it could be attributed to the initial state effect [19]. Taking into account that the framework of zeolites is negatively charged, one has to assign the observed shift in BE of Au4f to the electron transfer from the zeolite lattice to Au particles.

3.2.4. UV–vis

UV–vis spectroscopy is commonly used for identification of metallic gold and the nature of iron species in the catalysts. In line with XRD patterns, XPS results and TEM images, the UV–vis spectra confirm the presence of metallic gold on the surface of all gold and gold–iron zeolites (Fig. 3A and B). The UV–vis spectra of Au containing samples show the characteristic ultraviolet–visible band at 500 nm typical for metallic gold [20]. The small intensity bands between 200 and 280 nm visible in the spectra of all the samples are characteristic of the zeolite supports. They are attributed to a charge transfer due to Si–O bonding in zeolites and all silicates materials [21].

Fig. 3B displays the UV–vis spectra of gold–iron zeolites with strong absorbance in 200–800 nm range, revealing the existence of various iron species. In the spectrum of Au/Fe-ZSM-5 there are two well distinguished bands at 230 and 360 nm. They can be assigned to isolated Fe(III) in tetrahedral coordination and oligonuclear $Fe(III)_xO_y$ clusters on the zeolite external surface [22,23]. The isolated Fe(III) ions in tetrahedral coordination are present also in Au/Fe-Y and Au/Fe-Beta samples. Moreover, in the spectra of these zeolites two other bands at 280 and 320 nm are visible. These two bands are assigned to Fe(III) ions in octahedral coordination and to oligonuclear $Fe(III)_xO_y$ clusters on the zeolite internal surface, respectively [22,23]. The bands corresponding to $Fe(III)_xO_y$ clusters are the most intense for all three zeolites, showing high popula-

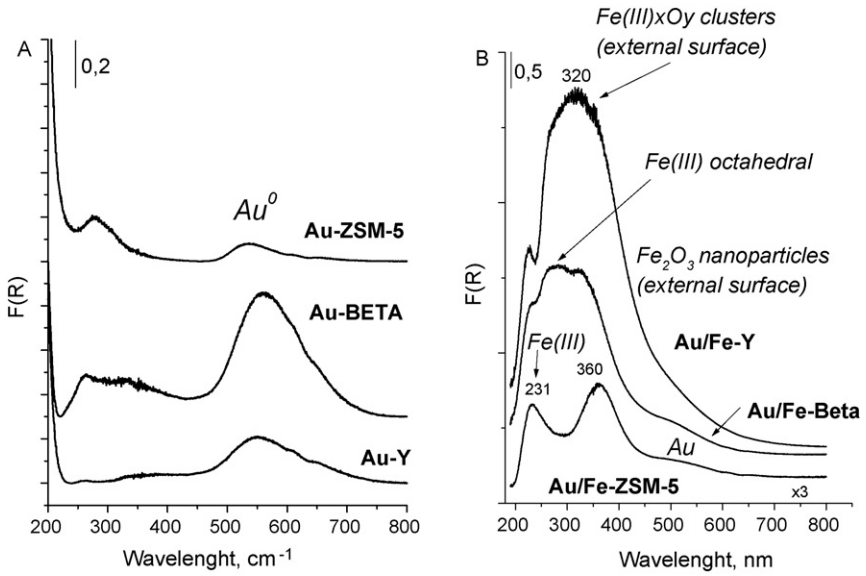

Fig. 3. UV–vis spectra of zeolites.

tion of iron oxides on the external (ZSM-5) or internal (Beta and Y) surface of zeolites after calcination.

3.3. Acidity/basicity

3.3.1. Test reactions

3.3.1.1. 2-Propanol decomposition. The 2-propanol decomposition is a test reaction for characterisation of acidic (Brönsted or Lewis) and/or basic properties of the solids [24]. Dehydration of alcohol to propene and/or diisopropyl ether requires acidic centres (Lewis or Brönsted), whereas the dehydrogenation to acetone occurs on the basic sites. It is noteworthy that ether production requires the presence of pairs Lewis acid–base centres. Some authors (e.g. [25]) have reported that acetone formation takes place on redox centres. The conversion of 2-propanol is much higher in the presence of acidic centres on the catalyst surface than that noted on basic catalysts.

As shown in Table 3 on all Au containing zeolites at 423 and 473 K the main reaction product is propene indicating the domination of acidic properties of the samples (Lewis or Brönsted). Additionally, for Au-ZSM-5 and Au/Fe-ZSM-5 zeolites small amount of diisopropyl ether was also recorded at 423 K among the reaction products, showing the presence of Lewis acid–base pairs beside acidic centres. Moreover, it is important to stress that at 473 K, acetone was identified on Au-Beta zeolite. Acetone is formed in dehydrogenation of alcohol, which occurs on Lewis basic centres.

Table 3
The results of 2-propanol decomposition at various temperatures.

Catalyst	React. temp. [K]	Conversion i-PrOH [%]	Selectivity [%] towards		
			Propene	Ether	Acetone
Au-Y	423	33	100	0	0
	473	100	100	0	0
Au/Fe-Y	423	67	100	Traces	0
	473	95	100	0	0
Au-Beta	423	78	84	13	3
	473	100	100	0	0
Au/Fe-Beta	423	44	100	Traces	0
	473	96	100	0	0
Au-ZSM-5	423	2	100	Traces	0
	473	33	76	24	0
Au/Fe-ZSM-5	423	16	72	28	0
	473	89	100	Traces	0

All the samples studied are highly acidic which is proved by their high activity and selectivity towards propene, alcohol dehydration product. It is understandable taking into account the treatment of all zeolites by auric acid during the modification with gold. The interaction with the acid leads to the formation of bridging acidic hyroxyls on the zeolite surface. However, diisopropyl ether and acetone were also found among the reaction products, especially on modified Beta and ZSM-5 type zeolites, which proved the presence of Lewis basic sites. Such centres most probably originate from extra framework iron-oxide species and dehydroxylated hydrogen forms of zeolites.

3.3.1.2. Acetonylacetone cyclisation. The cyclisation of acetonylacetone was used as a test reaction for basicity/acidity properties. This reaction was proposed by Dessau [26] as Brönsted acid–base test. The formation of 2,5-dimethylfuran (DMF) occurs on acidic centres, whereas basic centres take part in the production of 3-methyl-2-cyclopentenone (MCP). On the basis of the ratio of selectivity to MCP/selectivity to DMF, the catalysts prepared can be ordered according to increasing basicity. According to the literature [26,27] the catalyst is considered basic if MCP/DMF $\gg 1$. When MCP/DMF $\ll 1$ the catalyst exhibits acidic properties, while for MCP/DMF ≈ 1 the acid–base character of the catalysts is postulated.

The data on conversion of acetonylacetone (AcoAc) and selectivity towards DMF and MCP are given in Table 4. Hydrogen forms of Beta and ZSM-5 zeolites used as starting supports for modification with Au and Fe show 100% activity, whereas the activity of NaY is

Table 4
The results of acetonylacetone (AcoAc) cyclisation at 623 K.

Catalyst	Conversion (%)	DMF (%)	MCP (%)	MCP/DMF
NaY	14	92	8	0.1
Au-Y	30	98	2	0
Fe-Y	100	5	95	19
Au/Fe-Y	9	31	69	2.2
H-Beta	100	58	42	0.7
Au-Beta	45	100	0	0
Fe-Beta	100	48	52	1.1
Au/Fe-Beta	41	100	0	0
H-ZSM-5	100	100	0	0
Au-ZSM-5	63	100	0	0
Au/Fe-ZSM-5	70	100	0	0

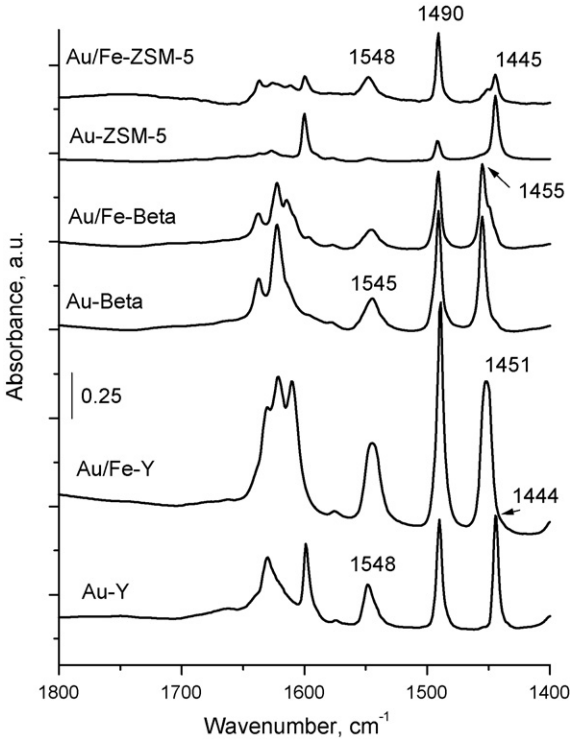

Fig. 4. FTIR spectra of zeolites after pyridine adsorption at 423 K and evacuation at 473 K.

much lower. The introduction of gold by deposition–precipitation and impregnation decreases the activity of H-Beta and H-ZSM-5 zeolites in AcoAc cyclisation as a result of gold introduction. In contrast, the modification of NaY with gold (Au-Y) generates new active centres and increases the activity of the catalyst. For all gold and gold–iron catalysts based on H-Beta and H-ZSM-5 zeolites DMF is the only product of the reaction which points to the acidic (Brönsted acid sites) character of these materials. Taking into account the activity of the gold-containing Beta and ZSM-5 samples, the Brönsted acidity of ZSM-5 based catalysts is higher than that of Beta-based zeolites. However, it is worthy of notice that H-Beta support reveals acid-base properties (MCP/DMF ~1) most probably caused by the presence of framework defects (LAS) on the surface appearing as a result of dehydroxylation of BAS. These defects most probably interact with water formed in the first step of AcoAc dehydration/cyclisation and form Brönsted basic OH groups active in MCP formation. Such defects are hardly formed after modification with Au and Fe because BAS present in the pristine zeolite supports (H-Beta and H-ZSM-5) interact with Fe and Au introduced.

Gold and gold–iron modified NaY catalysts show different features, both MCP and DMF products are formed in AcoAc cyclisation. The selectivity towards MCP is much higher for Au/Fe-Y than Au-Y (MCP/DMF > 1 for Au/Fe-Y). It seems probable that basicity originates from the extra framework iron-oxide species. The impregnation of basic Fe-Y (MCP/DMF = 19) with gold decreases the basicity indicating gold interaction with iron species, but gold–iron Y zeolite still exhibits basic character.

3.3.2. Pyridine adsorption

In order to evaluate the nature and amount of acidic centres, infrared spectroscopy (FTIR) of pyridine adsorbed was applied. Fig. 4 presents the ring stretching region of the FTIR spectra after adsorption of pyridine onto all gold and gold–iron zeolites and desorption at 473 K.

The spectra of the zeolites display six main bands. These bands can be ascribed to pyridine interacting with Brönsted and Lewis acid sites [28–30]. The bands at ca. 1450 and 1610 cm^{-1} are assigned to pyridine adsorbed at Lewis acid sites. The bands at ca. 1550 and 1620 cm^{-1} are due to pyridine adsorbed on Brönsted acidic hydroxyls, whereas the bands at ca. 1490 and 1637 cm^{-1} can be attributed to both Lewis and Brönsted acidity. Moreover, the small band at 1575 cm^{-1} is brought about by the presence of some residual physisorbed pyridine.

Fig. 4 shows different positions of the IR bands in the range of pyridine adsorbed on Lewis acid sites (1440–1455 cm^{-1}): 1444, 1451 and 1455 cm^{-1}. The band at 1444 cm^{-1} present in the spectra of Au-Y zeolite is assigned to the pyridine coordinatively bound to Na^+ cations [31]. The introduction of iron cations into NaY (over 90% of cation exchange) gives the band at 1451 cm^{-1} after pyridine adsorption attributed to the presence of iron cations in zeolite. The bands at 1451 and 1455 cm^{-1} observed for Au-ZSM-5 and Au-Beta zeolites, respectively, most probably originate from pyridine adsorbed on defected Lewis acid sites formed during dehydroxylation of hydrogen forms of zeolites. After cation exchange with iron the band at 1450 cm^{-1} assigned to pyridine adsorbed on iron cations appears (Au/Fe-Beta).

The intensity of the bands differs depending on the Si/Al ratio in zeolite and the amount of gold and iron in the sample and clearly increases with decreasing Si/Al ratio. The number of LAS and BAS for all zeolites studied is given in Table 5. The highest concentrations of Lewis and Brönsted acid sites are found in the Y samples. The high number of LAS in the form of Na cations significantly decreases after gold introduction. Gold species replace a part of Na cations in the zeolite and form the metallic sites after thermal treatment. On the other hand, the modification with gold generates BAS in Au-Y zeolite. The impregnation with gold of Fe-Y zeolite increases the number of LAS and decreases the number of BAS generated after Fe exchange. This phenomenon is caused by the calcination of Au/Fe-Y leading to dehydroxylation. The replacement of protons in H-Beta with gold species decreases the number of BAS, as well as LAS. The impregnation of Fe-Beta with gold leads to the blockade of part of Brönsted and Lewis acid sites and the number of acidic sites in Au/Fe-Beta decreases. ZSM-5 zeolite has the lowest number of LAS. Contrary to Y and Beta zeolites, it is clear that ZSM-5 modification with gold significantly increases the number of LAS. The strength of acidity can be deduced from the position of IR bands in the region 1600–1630 cm^{-1}. The higher wavenumber indicates the higher acidic strength. Examination of this region for Au/Fe-zeolites indicates the increase in wavenumber from 1610 to 1615 cm^{-1} for pyridine adsorbed on LAS and from 1621 to 1625 cm^{-1} for pyridine adsorbed on BAS in the following order: Au/Fe-Y < Au/Fe-

Table 5
Number of Brönsted acid sites (BAS) and Lewis acid sites (LAS) calculated per 10 mg of the catalysts on the basis of IR bands observed after desorption of pyridine at 473 K and extinction coefficient of pyridine (LAS $\varepsilon_{1450} \approx 1.5$ μmol^{-1} cm, BAS $\varepsilon_{1545} \approx 1.8$ μmol^{-1} cm).

Catalyst	Number of LAS × 10^{17}	Number of BAS × 10^{17}	Total number BAS + LAS × 10^{17}
NaY	21.00	–	21.00
Au-Y	9.75	5.05	14.8
Fe-Y	37.20	16.60	53.8
Au/Fe-Y	35.80	3.40	39.2
H-Beta	18.60	7.00	25.6
Au-Beta	13.40	4.58	17.98
Fe-Beta	19.80	6.63	26.43
Au/Fe-Beta	13.80	3.65	17.45
H-ZSM-5	1.39	11.50	12.89
Au-ZSM-5	6.05	0.70	6.75
Fe-ZSM-5	1.48	8.54	10.02
Au/Fe-ZSM-5	3.17	3.07	6.24

Table 6
The amount of Bu_2S adsorbed on examined materials.

Catalyst	wt.% of all adsorbates	wt.% of C	wt.% of H	wt.% of S	wt.% of Bu_2S	Selectivity [a] (%)
NaY	16.06	0.16	2.36	0	0	0
Au-Y	22.05	0.32	3.08	0.02	0.11	0.5
Fe-Y	2.99	1.38	2.66	0.21	0.98	32.6
Au/Fe-Y	11.32	1.44	2.47	0.34	1.58	13.9
Na-Beta	44.93	9.58	3.09	2.89	13.18	29.3
Au-Beta	17.84	7.95	2.28	2.41	10.98	61.6
Fe-Beta	17.55	8.36	2.46	2.63	12.00	68.4
Au/Fe-Beta	17.15	8.07	2.15	2.40	10.97	64.0
Na-ZSM-5	27.71	7.94	1.88	1.79	8.15	29.4
Au-ZSM-5	12.12	6.72	1.22	2.15	9.80	80.9
Au/Fe-ZSM-5	9.90	7.00	1.55	2.17	9.89	99.9

[a] Selectivity as the amount of Bu_2S in total amount of adsorbates.

Beta < Au/Fe-ZSM-5. This is the order of the strength of acidity of the zeolites studied.

3.4. Removal of odours

3.4.1. Adsorption of Bu_2S combined with the analysis by balance scale

The results of odours adsorption presented in Table 6 show a significant influence of the type of support on the amount of sulphide adsorbed and total adsorption.

The adsorption capacity of zeolites measured for all adsorbates (Bu_2S, moisture, CO_2 and others from air) depends on the type of zeolite (sodium form or zeolite after modification with Au and/or Fe), whereas the selective adsorption towards Bu_2S depends mainly on Si/Al ratio determining the hydrophilic/hydrophobic character of solids. The most hydrophilic sorbent, Y zeolite, preferentially adsorbs water, not dibutyl sulphide. The increase of Si/Al ratio decreases the hydrophilic character of the zeolite surface and the selectivity of Bu_2S adsorption increases. Among sodium forms of zeolites, the largest Bu_2S content in the total amount of adsorbates located in zeolite pores was noted for high silica zeolites (Na-Beta and Na-ZSM-5). The selectivity towards Bu_2S adsorption achieves 29 wt.% for these zeolites. The introduction of gold or gold together with iron strongly increases the sorption selectivity towards Bu_2S (ca. 60% and ca. 80% for Beta and ZSM-5 samples after modification, respectively). The odour adsorption for modified ZSM-5 zeolites reaches about 10 wt.%. Considering the amount of Bu_2S adsorbed, similar results were obtained on Beta-based samples (11–12 wt.% of Bu_2S adsorbed) but the selectivity of adsorption towards Bu_2S was much lower (62–68%). For Y zeolites the maximum amount of Bu_2S adsorbed was 1.5 wt.% on Au/Fe-Y, whereas on Au-Y it was only 0.1 wt.%. It indicates that the introduction of iron along with gold improves the sorption of sulphide in spite of almost two times higher total adsorption capacity indicated by Au-Y without iron. The role of iron in the selective adsorption of sulphide in the pores is evident for Au/Fe-Y and not so significant in Au/Fe-Beta and Au/Fe-ZSM-5. This behaviour should be related to the much higher amount of iron species in Y modified zeolite and the presence in it of iron-oxide species enhancing significantly Lewis acidity. According to increasing effectiveness for Bu_2S sorption, the zeolites studied can be ordered as follows:

$$\text{Fe-Beta} > \text{Au-Beta} \cong \text{Au/Fe-Beta} > \text{Au-ZSM-5} \cong \text{Au/Fe-ZSM-5} \gg \text{Au/Fe-Y} > \text{Au-Y}$$

The lowest Bu_2S sorption in modified Y zeolites, which are hydrophilic, is accounted for by the competition between the sorption of Bu_2S and that of moisture from the air.

The shapes of Bu_2S adsorption curves on selected catalysts are shown in Fig. 5. For the catalysts based on Y zeolite, very fast adsorption of all adsorbates (Bu_2S, moisture, CO_2 and others from air) takes place in the initial period after introduction of the first dose of dibutyl sulphide and a steady-state is reached. The second dose of Bu_2S does not cause a significant increase in the mass of the catalyst indicating that the zeolite cavities are already fulfilled. Interestingly, the rate of adsorption and the sorption capacity are much higher when Au-Y zeolite is used.

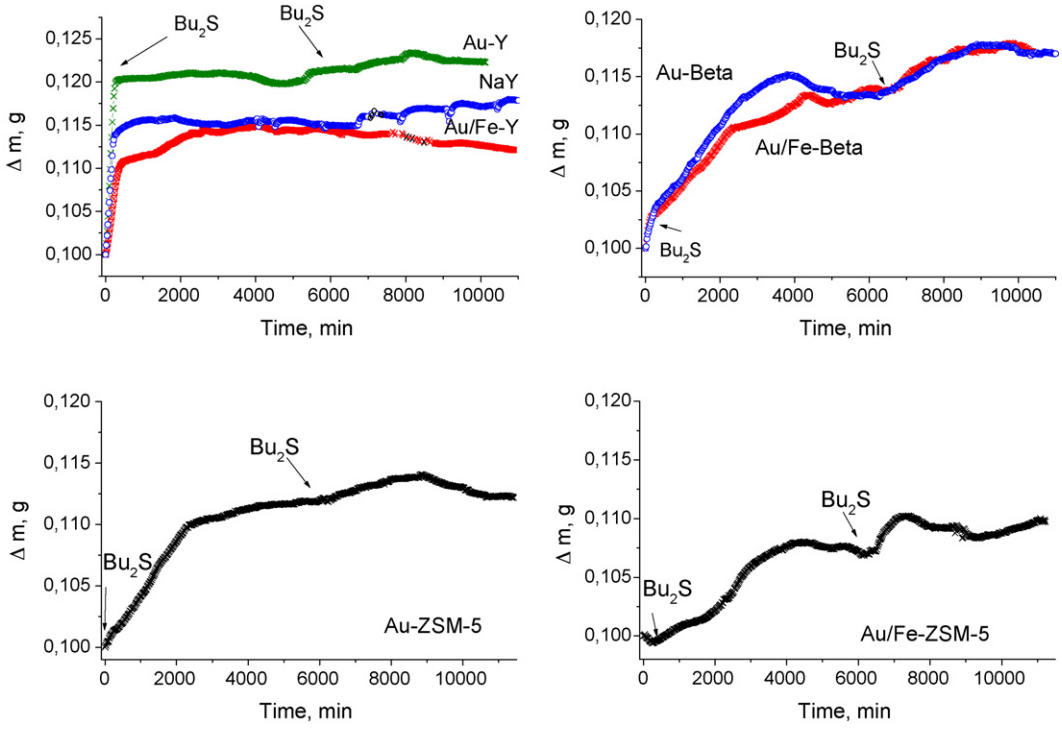

Fig. 5. Curves of air containing dibutyl sulphide adsorbed at room temperature.

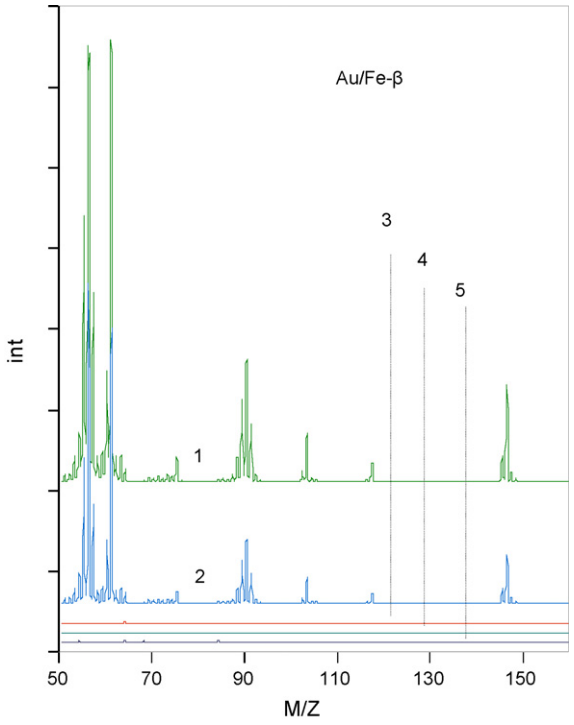

Fig. 6. Mass spectra of Au/Fe-β zeolite after Bu_2S adsorption at room temperature and evacuation at 363 K for 5 h: 1. phial with paint; 2. phial; 3. phial with paint—10 wt.% of Au/Fe-β; 4. phial with paint—20 wt.% of Au/Fe-β; 5. phial with paint—50 wt.% of Au/Fe-β.

Catalysts based on Beta and ZSM-5 zeolite adsorb dibutyl sulphide and other adsorbates slowly because of diffusion effects (exemplary curves Au-ZSM-5, Au/Fe-ZSM-5, Au-Beta and Au/Fe-Beta are shown in Fig. 5), and after introduction of the second dose of Bu_2S a distinct mass increase is noted. The shape of the adsorption curve shows some periodic losses of mass which could be explained by the desorption of Bu_2S caused by its migration in straight channels or by the desorption of products of Bu_2S catalytic transformation (oxidation).

3.4.2. Adsorption of Bu_2S combined with analysis by the electronic nose

Electronic nose can be applied to control and monitor odourants thanks to the capability of reproducing human senses using sensor arrays and pattern recognition systems [32]. In our study the electronic nose was used to detect Bu_2S or products of its oxidation.

To study the sorption capacity and the possible catalytic transformation of sulphide in practice, Au/Fe-Beta zeolite was admixtured with the paint. Au/Fe-Beta was selected for this study because of the highest amount of Bu_2S adsorbed on it and relatively high selectivity towards sulphide adsorption (64%). It is important to stress that the specific signals coming from dibutyl sulphide do not appear in the MS spectra of the contents of phials painted with the addition of the catalyst after desorption at 318 and 363 K (Fig. 6), whereas they were present in spectra recorded for nonpainted phials and those painted with pure paint (without the zeolite). The luck of Bu_2S in the atmosphere of phials painted by the mixture of chalk paint and desired zeolite indicates that sulphide is adsorbed in the zeolite added to the paint. This result proves strong adsorption of the model odourant on the surface of Au/Fe-Beta catalyst. One cannot exclude that the catalytic oxidation of adsorbed sulphide with oxygen from the air takes place on the surface of the paint with addition of Au/Fe-Beta. This point will be a subject of further study.

4. Discussion

The main aim of this work was to get insight into the possible use of modified zeolites for deodourisation of the air by adsorption and catalytic transformation of odours. Dibutyl sulphide (Bu_2S) was applied as a model compound representing odours containing sulphur as heteroatom. Taking into account the possible oxidation of sulphide adsorbed in the micropores of the zeolites, the modification of sorbents was performed with gold and iron species well known as active in catalytic oxidation.

The aim of this study was to estimate the effect of various parameters determining Bu_2S adsorption, such as: (i) zeolite structure, (ii) Si/Al ratio in the zeolites, responsible for hydrophobic/hydrophilic properties, (iii) acidity of the pristine and modified zeolites, (iv) transition metal modification. For this purpose we chose zeolites exhibiting various structures: cubic NaY containing large cavities (entrance to large cavities ~0.8 nm), Beta zeolite (hydrogen form) with two dimensional channels (6.6 nm × 6.7 nm and 5.6 nm × 5.6 nm), and ZSM-5 (hydrogen form) containing two systems of channels (5.1 nm × 5.5 nm and 5.3 nm × 5.6 nm). These zeolites were modified with gold and iron.

The adsorption curves of air containing Bu_2S (Fig. 5) indicated the role of the zeolite structure in the adsorption process. Cubic structure with cavities of Y type zeolites permitted the highest rate of adsorption evidenced by the shape of the adsorption curve. Much slower adsorption process was observed on Beta and ZSM-5 zeolites with channel structure and smaller size micropores than those in Y zeolites. The simplest interpretation of this phenomenon could be a diffusion effect leading to the decrease in the adsorption rate with decreasing micropore diameter (Y > Beta > ZSM-5). However, another point should be also considered. The rate at which the surface is covered by the adsorbate depends on the substrate's ability to dissipate the energy of the incoming molecule as it crushes onto the surface. The proportion of collisions with the surface that successfully lead to adsorption is called the sticking probability [*s*] and is expressed by: *s* = the rate of adsorption of molecules by the surface/the rate of collision of molecules with the surface [33]. The *s* value indicates how many collisions are needed before one molecule sticks successfully. It is known that the sticking probability on metal surfaces depends on the face of the metal crystal. One can postulate that the sticking probability depends on the shape of pores in non-metal solids and it is higher in the cavities than in the channels. Such explanation is in agreement with our previous observations [2,4] showing that adsorption of Bu_2S occurs very slowly in mesopores of MCM-41 materials containing parallel channels.

Considering odours adsorption one has to take into account the competition between moisture and odouring compound in diffusion and sorption inside pores of solids. Water is preferentially adsorbed on hydrophilic surfaces. The selectivity towards Bu_2S adsorption on sorbents used in this work clearly depends on the Si/Al ratio in the zeolites, determining the hydrophilic/hydrophobic character of solids (the higher Si/Al ratio in the zeolites the lower the hydrophilic character of the zeolite surface). The sorption selectivity towards Bu_2S (Table 6) increases in the order of Si/Al increase (Y-Si/Al = 2.7 < Beta-Si/Al = 12.5 < ZSM-5-Si/Al = 44.9). Moreover, when one considers the same type of zeolite, it should be noted that the selectivity towards Bu_2S adsorption is higher after modification of the zeolites with both metals (Au and Fe) in comparison with that of the samples modified by gold only. Iron admission into zeolites increases the number of acidic centres on the surface of zeolites. Dibutyl sulphide is chemisorbed on both Brönsted and Lewis acid centres. However, there is no simple relationship between the total number of acidic centres in all zeolites studied and the amount of Bu_2S adsorbed because the structural factor and hydrophilicity play a significant role.

The highest amount of Bu_2S was adsorbed in Beta zeolites and the experiment with painted phials and analysis with electronic nose indicated that the sulphide is strong adsorbed in the pores of Au/Fe-Beta, which gives hope for its possible regeneration via catalytic oxidation of sulphide.

5. Conclusions

- The structure of zeolites determines the rate of adsorption of the air containing Bu_2S. The presence of cavities in the zeolite structure permits higher adsorption rate than the presence of channels.
- Selectivity towards Bu_2S adsorption is determined by hydrophobicity of the samples, which increases with increasing Si/Al ratio in the zeolites (Y > Beta > ZSM-5).
- Within the same zeolite structures the selectivity towards Bu_2S adsorption increases with increasing total number of acidic centres. Iron modification of zeolites enhances the number of acidic sites.

Acknowledgements

Polish Ministry of Science (Grant No. N N204 032536) is acknowledged for the financial support of this work. Acknowledge is made also to Johnson Matthey (UK–USA) and Süd Chemie (Germany) for supplying $HAuCl_4$ and Beta and ZSM-5 zeolites, respectively.

References

[1] A. Callterieri, P.H. Thiesen, B. Niemeyer, Development of a basic procedure to design sorption processes, Waste Manage. 25 (2005) 985–993.
[2] M. Ziolek, I. Sobczak, A. Dudzik, B. Gorska, J. Kujawa, Application of modified zeolites and mesoporous materials for deodorization, Stud. Surf. Sci. Catal. 174 (2008) 555–560.
[3] M. Ziolek, I. Sobczak, A. Dudzik, L. Konwicki, J. Kujawa, Nanosorbents for selective removal of odours, Mater. Sci.-Pol. 26 (2008) 425–431.
[4] M. Ziolek, I. Nowak, H. Poltorak, A. Lewandowska, I. Sobczak, The possible use of mesoporous molecular sieves for deodorisation, Stud. Surf. Sci. Catal. 125 (1999) 691–698.
[5] J.-H. Chen, J.-N. Lin, Y.-M. Kang, W.-Y. Yu, Ch-N. Kuo, B.-Z. Wan, Preparation of nano-gold in zeolites for CO oxidation: effects of structures and number of ion exchange sites of zeolites, Appl. Catal. A: Gen. 291 (2005) 162–169.
[6] C. Baatz, N. Decker, U. Prüße, New innovative gold catalysts prepared by an improved incipient wetness method, J. Catal. 258 (2008) 165–169.
[7] Ch. Baerlocher, W.M. Meier, D.H. Olson, Atlas of Zeolitic Framework Types, 6th revised edition, Elsevier, 2007.
[8] N. Bogdanchikova, A. Simakov, E. Smolentseva, A. Pestryakov, M.H. Farias, J.A. Diaz, A. Tompos, M. Avalos, Stabilization of catalytically active gold species in Fe-modified zeolites, Appl. Surf. Sci. 254 (2008) 4075–4083.
[9] C. Kan, W. Cai, Z. Li, G. Fu, L. Zhang, Reduction effect of pore wall and formation of Au nanowires inside monolithic mesoporous silica, Chem. Phys. Lett. 382 (2003) 318–324.
[10] M. Iwasaki, K. Yamazaki, K. Banno, H. Shinjoh, Characterization of Fe/ZSM-5 DeNOx catalysts prepared by different methods: relationships between active Fe sites and NH_3-SCR performance, J. Catal. 260 (2008) 205–216.
[11] J.F. Moulder, W.F. Stickle, P.E. Sobol, K.D. Bomben, Handbook of X-ray Photoelectron Spectroscopy, Perkin–Elmer Corporation, Physical Electronics Division, Eden Prairie, 1992.
[12] I. Tuzovskaya, N. Bogdanchikova, A. Simakov, V. Gurin, A. Pestryakov, M. Avalos, M.H. Farias, Structure and electronic states of gold species in mordenites, Chem. Phys. 338 (2007) 23–32.
[13] P. Lignier, M. Comotti, F. Schuth, J.-L. Rousset, V. Caps, Effect of the titania morphology on the Au/TiO_2-catalyzed aerobic epoxidation of stilbene, Catal. Today 141 (2009) 355–360.
[14] G.M. Veith, A.R. Lupini, S.J. Pennycook, G.W. Ownby, N.J. Dudney, Nanoparticles of gold on γ-Al_2O_3 produced by dc magnetron sputtering, J. Catal. 231 (2005) 151–158.
[15] A.Q. Wang, J.H. Liu, S.D. Linb, T.S. Lin, C.Y. Mou, A novel efficient Au–Ag alloy catalyst system: preparation, activity, and characterization, J. Catal. 233 (2005) 186–197.
[16] P. Konova, A. Naydenov, C.D. Venkov Mehandjiev, D. Andreeva, T. Tabakova, Activity and deactivation of Au/TiO_2 catalyst in CO oxidation, J. Mol. Catal. A 213 (2004) 235–240.
[17] S. Arrii, F. Morfin, A.J. Renouprez, J.L. Rousset, Oxidation of CO on gold supported catalysts prepared by laser vaporization: direct evidence of support contribution, J. Am. Chem. Soc. 126 (2004) 1199–1205.
[18] F.-W. Chang, H.-Y. Yu, L.S. Roselin, H.-C. Yang, T.-Ch. Ou, Hydrogen production by partial oxidation of methanol over gold catalysts supported on TiO_2–MOx (M = Fe, Co, Zn) composite oxides, Appl. Catal. A 302 (2006) 157–167.
[19] J. Radnik, C. Mohr, P. Claus, On the origin of binding energy shifts of core levels of supported gold nanoparticles and dependence of pretreatment and material synthesis, Phys. Chem. Chem. Phys. 5 (2003) 172–177.
[20] D.L. Feldheim, C.A. Foss, Metal Nanoparticles. Synthesis, Characterization and Applications, Basel Marsel Dekker, Inc., New York, 2002.
[21] R. Diaz, D. Lopez-Gallo, Spectroscopic characterization of Co, Cu, Cd catalysts supported on Si–Al–Y Zeolite sol–gel matrix, React. Kinet. Catal. Lett. 65 (1998) 67–73.
[22] J. Perez-Ramirez, J.C. Groen, A. Bruckner, M.S. Kumar, U. Bentrup, M.N. Debbagh, L.A. Villaescusa, Evolution of isomorphously substituted iron zeolites during activation: comparison of Fe-beta and Fe-ZSM-5, J. Catal. 232 (2005) 318–334.
[23] L. Li, Q. Shen, J. Li, Z. Hao, Z. Ping Xu, G.Q. Max Lu, Iron-exchanged FAU zeolites: preparation, characterization and catalytic properties for N_2O decomposition, Appl. Catal. A: Gen. 344 (2008) 131–141.
[24] A. Gervasisni, J. Fenyvesi, A. Auroux, Study of the acidic character of modified metal oxide surfaces using the test of isopropanol decomposition, Catal. Lett. 43 (1997) 219–228.
[25] C. Lahousse, J. Bachelier, J.C. Lavalley, H. Lauron-Pernot, A.M. Le Govic, Validity of using isopropanol decomposition as a test-reaction for the characterization of metal oxides basicity; comparison with results obtained from methylbutynol decomposition, J. Mol. Catal. 87 (1994) 329–332.
[26] R.M. Dessau, Base- and acid-catalysed cyclization of diketones over ZSM-5, Zeolites 10 (1990) 205–206.
[27] J.J. Alcaraz, B.J. Arena, R.D. Gillespie, J.S. Holmgren, Solid base catalysts for mercaptan oxidation, Catal. Today 43 (1998) 89–99.
[28] S. Khabtou, T. Chevreau, J.C. Lavalley, Quantitative infrared study of the distinct acidic hydroxyl groups contained in modified Y zeolites, Micropor. Mater. 3 (1994) 133–148.
[29] E.P. Parry, An infrared study of pyridine adsorbed on acidic solids. Characterization of surface acidity, J. Catal. 2 (1963) 371–379.
[30] O.M. Busch, W. Brijoux, S. Thomson, F. Schüth, Spatially resolving infrared spectroscopy for parallelized characterization of acid sites of catalysts via pyridine sorption: possibilities and limitations, J. Catal. 222 (2004) 174–179.
[31] M.R. Basila, T.R. Kantner, K.H. Rhee, The nature of the acidic sites on a silica-alumina. Characterization by infrared spectroscopic studies of trimethylamine and pyridine chemisorption, J. Phys. Chem. 68 (1964) 3197–3207.
[32] S. Ampuero, J.O. Bosset, The electronic nose applied to dairy products: a review, Sens. Actuators B 94 (2003) 1–12.
[33] P.W. Atkins, Physical Chemistry, Oxford University Press, 1992.